HHS Public Access

Author manuscript

Acta Biomater. Author manuscript; available in PMC 2016 July 01.

Published in final edited form as:

Acta Biomater. 2015 July 1; 20: 22–31. doi:10.1016/j.actbio.2015.04.004.

Silk scaffolds with tunable mechanical capability for cell differentiation

Shumeng Bai[a,b], **Hongyan Han**[c,#], **Xiaowei Huang**[a,b], **Weian Xu**[c], **David L. Kaplan**[a,d], **Hesun Zhu**[e], and **Qiang Lu**[a,b,*]

[a]National Engineering Laboratory for Modern Silk & Collaborative Innovation Center of Suzhou Nano Science and Technology, Soochow University, Suzhou 215123, People's Republic of China

[b]College of Textile and Clothing Engineering, Soochow University, Suzhou 215123, People's Republic of China

[c]School of Biology and Basic Medical Sciences, Soochow University, Suzhou 215123, People's Republic of China

[d]Department of Biomedical Engineering, Tufts University, Medford, MA02155, USA

[e]Research Center of Materials Science, Beijing Institute of Technology, Beijing100081, People's Republic of China

Abstract

Bombyx mori silk fibroin is a promising biomaterial for tissue regeneration and is usually considered an "inert" material with respect to actively regulating cell differentiation due to few specific cell signaling peptide domains in the primary sequence and the generally stiffer mechanical properties due to crystalline content formed in processing. In the present study, silk fibroin porous 3D scaffolds with nanostructures and tunable stiffness were generated via a silk fibroin nanofiber-assisted lyophilization process. The silk fibroin nanofibers with high β-sheet content were added into the silk fibroin solutions to modulate the self-assembly, and to directly induce water-insoluble scaffold formation after lyophilization. Unlike previously reported silk fibroin scaffold formation processes, these new scaffolds had lower overall β-sheet content and softer mechanical properties for improved cell compatibility. The scaffold stiffness could be further tuned to match soft tissue mechanical properties, which resulted in different differentiation outcomes with rat bone marrow-derived mesenchymal stem cells towards myogenic and endothelial cells, respectively. Therefore, these silk fibroin scaffolds regulate cell differentiation outcomes due to their mechanical features.

*Corresponding author: Qiang Lu, Tel: (+86)-512-67061649; Lvqiang78@suda.edu.cn.
#The author has same contribution with the first author

Keywords

silk fibroin; nanofibrous scaffolds; cell differentiation; tissue engineering

1. Introduction

Tissue engineering has stimulating the development of biomaterial scaffolds with tuned properties to satisfy the requirements of specific tissue regeneration, and to actively regulate cell behaviors [1-5]. Aside from specific peptide epitopes, scaffold morphology and topology, crystallinity and stiffness are amongst the parameters that influence the cell behavior, extracellular matrix production and functional tissue reconstruction [6-10]. Recently, silk fibroin, a fibrillar protein, has attracted attention for support matrices for stem cells, nerve cells, fibroblasts, osteoblasts and other cell types, as well as scaffolds for many different types of tissues for engineering, including skin, nerve, bone, cartilage and blood vessels [11-15]. These studies were prompted in part due to the impressive biocompatibility, unique mechanical properties, tunable biodegradability and minimal inflammatory reactions with silk fibroin [16-20].

Biomimetic nanostructures are an emerging strategy in designing scaffolds with better biocompatibility [21-25]. Electrospinning, an effective way to prepare biomimetic nanofibrous structures was used to generate silk fibroin sheets and tubes [26-29], but is a difficult approach to generate scaffolds with microporous structures (pore size >100μm) and sufficient thickness for bone, cartilage, liver or muscle regeneration as examples [30,31]. Other processing options, such as salt leaching and freeze-drying, could be used to design complex three dimensional (3-D) microporous silk fibroin scaffolds [32-34], but do not generate biomimetic nanostructures.

Different approaches and post-treatment processes have been developed to control the crystallinity of silk fibroin scaffolds [35-37]. Although some improvements were achieved, softening the water-insoluble scaffolds to match the requirements of different soft tissues is difficult since the high crystallization, a prerequisite for water-insolubility of silk fibroin scaffolds, usually results in higher stiffness [35,36]. Therefore, silk fibroin scaffolds are once considered “inert” matrices with respect to directing cell differentiations [8]. Recently, a self-assembly mechanism to control silk fibroin nanofiber formation in aqueous solution was reported [38,39] and 3-D porous silk fibroin scaffolds composed of nanofibers were successfully prepared using a lyophilization process [40-42]. However, the nanofibrous architectures are usually occluded, thus failing to directly interact with cells seeded on these matrices. Post-treatment processes such as methanol annealing were required to achieve water insolubility of the scaffolds, causing an increase in stiffness [41,42]. Silk fibroin nanofibers with high beta-sheet structure were prepared in our recent study [43]. Unlike previous water-insoluble silk fibroin materials with high beta-sheet content [33,41], these nanofibers could be homogeneously dispersed in water to form stable solutions, thus serving an inducer of silk fibroin nanostructures with control of conformational transformations.

Therefore, in the present study, silk fibroin nanofibers were used to induce nanofiber growth and conformational transformations in fresh silk fibroin solutions to generate biomimetic

nanofibrous/microporous silk fibroin scaffolds with tunable stiffness. The insoluble regenerated silk fibroin scaffolds were prepared directly from aqueous solution without the use of any additives or post-treatments, avoiding higher stiffness and higher crystallinity formation. Scaffold stiffness and nano-topography could be tuned by changing the nanofiber content in the fresh solution before lyophilization, and then provide stimulating cues to actively influence stem cell growth and differentiation so that silk fibroin is a useful option for soft tissue studies.

2. Experimental section

2.1 Preparation of aqueous silk fibroin solutions

Silk fibroin solution was prepared according to our previously described methods [38]. *Bombyx mori* cocoons were boiled for 20 min in an aqueous solution of 0.02 M Na_2CO_3, and then rinsed thoroughly with distilled water to extract the sericin proteins. The degummed silk was dissolved in 9.3 M LiBr solution at 60°C, yielding a 20% (w/v) solution. This solution was dialyzed against distilled water, using a dialysis tube (MWCO 3,500, Pierce, Rockford, IL, USA) for 72 h to remove the salt. The solution was optically clear after dialysis and was centrifuged at 9,000 rpm for 20 min at 4°C to remove silk fibroin aggregates formed during the process. The final concentration of aqueous regenerated silk fibroin solution was about 6 wt%, determined by weighing the remaining solid after drying.

2.2 Preparation of silk fibroin nanofiber solutions

The silk fibroin nanofiber was assembled as reported in our recent study [43]. Fresh silk fibroin solution was treated by a concentration-dilution process. The solution (6 wt%) was slowly concentrated to about 20 wt% over 24 h at 60°C to form metastable nanoparticles, and then diluted to 0.5 wt% with distilled water. The diluted silk fibroin solution was incubated for above 24 h at 60°C to induce the nanofiber formation.

2.3 Preparation of silk fibroin scaffolds

Silk fibroin scaffolds were prepared via a modified lyophilization method. The fresh silk fibroin solution was blended with the silk fibroin nanofiber solution at dry weight ratios (silk: silk nanofiber) of 100: 0, 98: 2, 93.7: 6.3, 88.2: 11.8, and 66.7: 33.3, respectively. The blend silk fibroin solutions were diluted to 2 wt% with distilled water, and then poured into cylindrically-shaped containers. The containers were placed at -20°C for 24 h to freeze the samples, which were then lyophilized for about 72 h. After lyophilization the scaffolds were prepared and termed SS-0, SS-2, SS-6.3, SS-11.8, and SS-33.3, respectively. Since the soluble ingredient could be removed within 12 h based on the residual mass (%) results (Fig. 1), the regenerated silk fibroin scaffolds were immersed in distilled water at 37°C for 12h to remove any residual soluble silk fibroin to achieve final scaffolds with biomimetic nanostructures and tunable stiffness.

2.4 Morphological structure of the scaffolds

The morphology of the scaffolds was observed using a scanning electron microscopy (SEM, Hitachi S-4800, Hitachi, Tokyo, Japan) at 3 kV. Samples were mounted on a copper plate and sputter-coated with gold prior to imaging. The pore diameters of scaffolds were

measured using Image J software. Above 300 different sites for every sample were measured and then the average values were achieved.

2.5 Structural analysis of the scaffolds

The structure of the different scaffolds was analyzed by Fourier transform infrared spectroscopy (FTIR) on a Nicolet FTIR 5700 spectrometer (Thermo Fisher Scientific, Waltham, MA, USA). For each measurement, 64 scans were coded with a resolution of 4 cm^{-1}, with the wavenumber ranging from 400 to 4000 cm^{-1}. Fourier self-deconvolution (FSD) of the infrared spectra covering the amide I region (1595-1705 cm^{-1}) was performed by Peakfit 4.12 software to identify silk secondary structures [44]. FSD spectra were curve-fitted to measure the relative areas of the amide I region components. The crystal structure of the scaffolds was confirmed with X-ray diffraction (XRD, X′ Pert-Pro MPD, PANalytical B V, Almelo, Netherlands) using monochromated CuKa radiation (30 mA, 40kV) with a scanning speed of 0.6°/min.

2.6 Mechanical properties

The compressive properties of the samples in wet state were measured using an Instron 3366 testing frame (Instron, Norwood, MA, USA) with a 10 N capacity load cell [33,41]. The cylinder-shaped scaffolds (10 mm in diameter and 20 mm in height) were hydrated in water for 2 h and then measured with a cross head speed of 2 mm min^{-1} at 25°C and 65% RH. The load was applied until the cylinder was compressed by more than 30% of its original length. The compressive modulus was calculated as the slope of the linear region of the stress-strain curve. All samples were measured in triplicates.

2.7 *In vitro* biocompatibility of the scaffolds

Bone marrow mesenchymal stem cells (BMSCs) derived from Sprague-Dawley (SD) rats were used to evaluate the *in vitro* biocompatibility of the scaffolds via DNA content assay, fluorescence staining and SEM, respectively [40]. The scaffolds were punched into small disks (diameter of 5 mm and height of 2 mm) for 96-well plates and sterilized with ^{60}Co γ-irradiation at the dose of 25 kGy. BMSCs were cultured in Dulbecco's modified Eagle medium (DMEM, low glucose) supplemented with 10% fetal bovine serum (FBS), and 1% IU ml^{-1} streptomycin-penicillin (Invitrogen, Carlsbad, CA, USA). The medium was replaced every 3 days, and the cultures were maintained in a humidified incubator at 37°C and 5% CO_2. After reaching 90% confluence, cells were detached from Petri dish and seeded into the scaffolds at a density of 1.0×10^5 per well.

The cell morphology on the scaffolds was examined by confocal microscopy. After culture for 1, 6, and 12 days, the cell-seeded scaffolds were washed three times with PBS and fixed in 4% paraformaldehyde (Sigma-Aldrich, St Louis, MO, USA) for 30 min, followed by further washing. The cells were permeabilized with 0.1% Triton X-100 for 5 min and incubated with FITC-phalloidin (Sigma-Aldrich, St. Louis, MO, USA) for 20 min at room temperature, followed by washing with PBS and, finally, staining with DAPI (Sigma-Aldrich, St. Louis, MO, USA) for 1 min. Representative fluorescence images of stained samples were obtained using a confocal laser scanning microscope (FV10 inverted microscope, Olympus, Nagano, Japan) with excitation/emission at 358/462 nm and 494/518

nm. The images of the scaffolds were captured from the surface to a depth of 100 μm in increments of 10 μm. The cell morphology on the scaffolds was confirmed by SEM. After harvest the cell-seeded scaffolds were washed three times with PBS, fixed in 4% paraformaldehyde at room temperature, and then again washed three times with PBS. Fixed samples were dehydrated through a gradient of alcohol (50%, 70%, 80%, 90%, 100%, 100%) followed by lyophilization. After coated with gold, the samples were examined with SEM at the voltage of 3 kV. Several different areas of the specimens were randomly examined using a model S-4800 SEM (Hitachi, Tokyo, Japan).

To study cell proliferation on the scaffolds, samples were harvested at the indicated time points (from 1 to 12 d) and digested with proteinase K overnight at 56°C, as described previously [40]. The DNA content was determined using the PicoGreen™ DNA assay following the protocol of the manufacturer (Invitrogen, Carlsbad, CA, USA). The DNA content was measured at an excitation wavelength of 480 nm and emission wavelength of 530 nm using a BioTeK Synergy 4 spectrofluorometer (BioTeK, Winooski, VT, USA). The amount of DNA was calculated by interpolation from a standard curve prepared with λ-phage DNA in 10×10^{-3} M Tris-HCl (pH 7.4), 5×10^{-3} M NaCl, 0.1×10^{-3} M EDTA over a range of concentrations.

2.8 *In vitro* cell differentiation on the scaffolds

In order to clarify the effects of biomaterial stiffness on the differentiation of BMSCs, the levels of Desmin, Myogenesis Differentiation Protein 1(MyoD1), Vascular endothelial growth factor receptor 1 (Flt-1), Kinase insert domain protein receptor (Kdr) and glyceraldehydes-3-phosphate dehydrogenase (GAPDH) genes were studied via quantitative real-time PCR (qRT-PCR) after 1, 7, 14 and 28 days of culture, respectively [3,45-47]. Total cellular RNA from each sample was extracted with Trizol reagent (Invitrogen, Carlsbad, CA, USA). RNA extracts were converted into complementary DNA (cDNA) using a High-Capacity cDNA Reverse Transcription kit (Applied Biosystems, Carlsbad, CA, USA) in a 2720 thermal cycler (Applied Biosystems, Foster City, CA, USA). Quantitative real-time PCR was performed in a 7500 Real-Time PCR System (Applied Biosystems, Foster City, CA, USA) with the Fast SYBR Green kit (Applied Biosystems, Carlsbad, CA, USA). The sequences of primers were given in Table 1. The mRNA expression level of Desmin, MyoD1, Flt-1, Kdr and GAPDH was expressed as threshold cycle (CT) values, and the expression of the house keeping gene GAPDH was used as internal control to normalize results. The comparative Ct-value method was used to calculate the relative expression. Each sample was analyzed in triplicate.

Immunofluorescence staining of cells with MyoD1 (myogenic cell marker) and CD31 (endothelial cell marker) was used to characterize myogenic and endothelial differentiation of BMSCs [3,48,49]. Briefly, the samples were washed with PBS, fixed with 4% paraformaldehyde (Sigma-Aldrich, St. Louis, MO, USA) for 30 min, followed by permeabilization with 1% Triton X-100 for 30 min and blocked with 3% rabbit for 30 min at room temperature. Then, samples were incubated with mouse anti-MyoD1 primary antibody (1:100, Santa Cruz, Dallas, TX, USA) and mouse anti-CD31 primary antibody (1:100, Santa Cruz, Dallas, TX, USA) overnight at 4°C, respectively. After washing three times with PBS,

samples were incubated with goat anti-mouse IgG secondary antibody (1:500, Invitrogen, Carlsbad, CA, USA) for 60 min before incubation with DAPI (Sigma-Aldrich, St. Louis, MO, USA) for 3 min. Representative fluorescence images of stained samples were obtained by confocal laser scanning microscopy (CLSM, FV10 inverted microscope, Olympus, Nagano, Japan).

2.9 Statistical analysis

All statistical analyses were performed using SPSS v.16.0 software. Comparison of the mean values of the data sets was performed using two-way ANOVA. Measures are presented as means ± standard deviation, unless otherwise specified, and $P < 0.05$ was considered significant.

3. Results and Discussion

3.1 Morphology and structure of silk fibroin scaffolds

A feasible approach to the preparation of biomimetic nanofibrous silk fibroin scaffolds with nanofibers as inducer in lyophilization process has been shown [40-41]. The silk fibroin nanofibers with diameter of about 20 nm could induce further silk fibroin nanofiber assembly in lyophilization, resulting in scaffold formation with nanofibrous structures. The nanofibrous structures concealed on the scaffold wall showed nanoparticle topography firstly and then emerged following degradation process. Although metastable silk fibroin nanofibers were prepared in aqueous solution to improve the microstructure of silk fibroin freeze-dried scaffolds, the nanofibers tend to transform into silk II structure, resulting in precipitation formation before lyophilization and then the failure of scaffold preparation [38,39]. Stable silk fibroin nanofibers with high beta-sheet content have been achieved by regulating the self-assembly process (Fig. S1) [43]. In contrast to previous silk II-rich materials [39,50], the nanofibers have a higher zeta potential (above -50 mV), which provides sufficient charge repulsion to restrain further aggregation. Therefore, the silk fibroin nanofibers could be stably dispersed in aqueous solution and homogeneously blend with fresh silk fibroin solution to induce further nanofiber growth during the lyophilization process.

The water stability of the scaffolds was improved following increased nanofibers added (Fig. 1). The insoluble fraction of the scaffolds was 40% and 72% when the nanofiber content was 2% and 6.3%, and exceeded 90% when the nanofiber content was above 11.8%. The improvement in stability could be attributed to the nanofiber-induced silk II formation in the lyophilized scaffolds. Structural changes of the silk fibroin scaffolds following nanofiber additions and the removal of the soluble fraction of silk fibroin were investigated by FTIR (Fig. 2A). The infrared spectral region within 1700-1600 cm^{-1}, assigned to absorption by the peptide chains of amide I, is usually used for the analysis of different secondary structures of silk fibroin. The peaks at 1648-1652 cm^{-1} and 1635-1645 cm^{-1} are indicative of silk I conformation and random coil, respectively, while the peaks at 1610-1630 cm^{-1} are characteristic of silk II conformation [33,40,42]. Before the removal of soluble silk fibroin, except for the scaffolds containing 33.3% nanofiber, all of the scaffolds had a broad peak at 1644 cm^{-1}, corresponding to random coil. FSD of the infrared spectra in

the amide I (1595-1705 cm^{-1}) region indicated that the beta-sheet content increased slightly from 16.6% to 20.3%, 24.9%, 28.3%, 32.3% in the SS-2, SS-6.3, SS-11.8 and SS-33.3 scaffolds, respectively (Table 2). These results suggested that the nanofibers could induce slight beta-sheet formation in the lyophilization process. After the removal of soluble silk fibroin fraction, the silk I and silk II peaks appeared in the spectra of the SS-6.3 and SS-11.8 scaffolds, while the silk II peak was significantly enhanced for the SS-33.3 scaffolds, accompanied by the disappearance of random coil peaks because the soluble silk fibroin is mainly composed of random structure. Comparing with methanol treated scaffolds, these water-insoluble nanofiber-regulated scaffolds had reduced silk II content and achieved various secondary structure compositions for tunable properties. XRD further confirmed the structural changes of these scaffolds (Fig. 2B). Before the removal of soluble fractions, the SS-0, SS-2, SS-6.3 and SS-11.8 scaffolds had a broad peak between 10 to 35°, the indicative of an amorphous phase. Typical silk I and silk II peaks appeared in the curves of the SS-6.3, SS-11.8 and SS-33.3 scaffolds after the removal of the soluble fraction of silk fibroin where the strength of silk II peaks was significantly lower than that found with methanol treated scaffolds. Both the FTIR and XRD results suggested that silk fibroin nanofiber-assisted lyophilization was a feasible way to tune the secondary structure of water-insoluble silk fibroin scaffolds with reduced silk II content.

The microstructure and topography of these silk fibroin scaffolds were revealed with SEM. Similar to previous study [40], the nanofibers could facilitate microporous structure formation in lyophilization process (Fig. 3). By adding silk fibroin nanofibers in the aqueous solution, the microstructures of scaffolds gradually changed from lamellar (SS-0) to interconnected porous structures with a pore diameter of 250 ± 60 μm (SS-11.8 and SS-33.3). Following the increase of the added nanofibers, the topography became more pronounced and changed into nanoparticle structure after the removal of the soluble silk fibroin fraction. Similar to previous study [41], the nanoparticles were derived from the formed nanofibers that could emerge after degradation (Fig. S2). Interestingly, the silk fibroin scaffolds were mainly composed of nanofiber structures when the content of the added nanofibers was above 6.3% (the weight content in dry scaffold), suggesting that the added nanofibers induced random silk fibroin chains in solution to form nanofibers during the lyophilization process, similar to what happened in collagen/silk composite scaffolds [30]. Therefore, silk fibroin nanofibers with high beta-sheet content elicited conformational and nanostructural transitions of silk fibroin in fresh solution and resulted in the formation of biomimetic nanofibrous/microporous silk fibroin scaffolds with reduced silk II structure. Silk fibroin in aqueous solution is metastable and gradually transforms into β-sheet structure, resulting in hydrogel formation [43]. Previous studies in our group have found that the transformation process was regulated by different factors such as temperature, concentration and hydrophic/hydrophobic interactions [38]. Since lower molecular motility at lower temperate restrains the transformation, the lyophilized silk fibroin scaffolds are usually soluble and mainly composited of amorphous states. In our group, it was found that the silk nanofibers with high β-sheet content could accelerate the transformation process, and then induce hydrogel formation in shorter time. Therefore, the nanofibers were added into fresh silk fibroin solution to facilitate silk fibroin transformation in lyophilization. The

water-insoluble scaffolds with tunable β-sheet content were directly prepared without further post-treatment through adjusting the nanofiber content.

3.2Mechanical properties of silk scaffolds

The insoluble silk fibroin nanofiber-regulated scaffolds showed different mechanical properties in the hydrated state (Table 3). Although the beta-sheet content in the scaffolds increased following the increase of added nanofibers, the modulus was 6 kPa for SS-6.3 scaffolds and increased to 16 kPa for SS-11.8 scaffolds, but decreased to 5 kPa for SS-33.3 scaffolds. The decrease of stiffness with higher beta-sheet content was reasonable since the incremental charge repulsion of the added nanofibers could restrain the aggregation of silk fibroin, similar to what happened in silk fibroin nanofiber hydrogel systems [39,43,44]. The silk fibroin nanofiber-regulated scaffolds had significantly softer mechanical properties compared with previously reported methods [33,41], offering tunable stiffness similar to muscle or endothelial tissues [3,46, 51].

3.3 *In vitro* Biocompatibility

BMSC attachment and proliferation were used to evaluate cell compatibility of the scaffolds. Methanol-treated silk fibroin scaffolds (MT-SS-0) prepared from fresh silk fibroin solution were used as a control to assess the influence of nanofibrous structure on cell behavior [41]. Fig. 4 shows typical cell attachment and growth on different silk fibroin scaffolds. BMSCs grew well on all the scaffolds from day 1 to 12. Fluorescence staining confirmed cell viability and attachment throughout all scaffolds. At day 12, cells proliferated significantly, filled the pore spaces and formed a continuous monolayer on the scaffolds. Significantly better cell growth was achieved on the nanofibrous scaffolds (SS-6.3 and SS-11.8) than on the methanol treated scaffolds. SEM results confirmed the better growth on the nanofibrous scaffolds (Fig. 5). More cell-ECM monolayer structures formed on the surface of the nanofibrous scaffolds, implying that the nanofibrous silk fibroin scaffolds with good porous structures showed significantly better cell compatibility. DNA assay revealed that cell numbers on the scaffolds increased up to 12 days without reaching a plateau and higher cell numbers were achieved on the nanofibrous silk fibroin scaffolds (Fig. 5G). Considering that the adhered cells on the two scaffolds at day 1 were similar, the higher cell numbers on the SS-6.3 and SS-11.8 scaffolds indicated better cell growth on the nanofibrous scaffolds. These results revealed that the scaffolds with good porous structure and nanofibrous topography showed better biocompatibility than the scaffolds from fresh regenerated silk fibroin solution. Some studies have revealed that ECM-mimic nanofibrous topography and porous structures could provide a better microenvironment for cells [30,40,52,53]. Although it is impossible to clarify the specific actions of microporous and nanofibrous structures in improving the biocompatibility, the cell culture results suggested an improved biocompatibility of the scaffolds containing silk nanofibers.

3.4 Tunable differentiation of BMSCs

Recent studies have demonstrated the effect of matrix stiffness on the differentiation of MSCs [3,9,54,55]. Although silk fibroin scaffolds have been used in different studies of tissue regeneration [11-15], it remains a challenge to fabricate silk fibroin scaffolds with stiffness that could match different soft tissues. In our present study, silk fibroin nanofibers

as an inducer were used to regulate the nanostructure and crystallization of the water-insoluble lyophilized silk fibroin scaffolds to prepare scaffolds with reduced stiffness. The modulus of SS-11.8 and SS-6.3 scaffolds was 16.7kPa and 6.2 kPa, respectively, similar to that of native muscle and endothelial cells [3,46,51]. These data suggest the possibility of actively inducing the differentiation behavior of stem cells to muscle and endothelial cells on the corresponding scaffolds.

The myogenic differentiation of BMSCs was assessed by qRT-PCR for key myogenic lineage-specific markers (Desmin and MyoD1) (Fig. 6A and B). The expression of Desmin, which is an early marker of myogenic differentiation [56,57], was highest at 7 days and then decreased at 14 and 28 days on the SS-11.8 scaffolds (Fig. 6A). The down-regulation of Desmin after 7 days is related to the cellular switching process into next myogenic steps. The mRNA expression of MyoD1, a critical marker of myogenic differentiation [3], was also investigated, which showed sustainable increase on SS-11.8 scaffolds over time (Fig. 6B). In contrast, the myogenic specific markers remained significantly lower in terms of gene expression after 28 days on the methanol-treated silk fibroin scaffolds and SS-6.3 scaffolds. Immunofluorescent staining was also undertaken to detect MyoD1 expression (Fig. 6E). Significantly stronger expression appeared on SS-11.8 scaffolds, confirming the preferred differentiation to muscle cells on the SS-11.8 scaffolds with stiffness that could match muscle tissue [3,51].

Considering that the SS-6.3 scaffolds had similar stiffness with *in vivo* intima basement membrane of native blood vessels [46,58], it was deduced that preferred differentiation into endothelial cells could be considered on the scaffolds. The endothelial differentiation of BMSCs was studied with key endothelial markers (Kdr and Flt-1) on the SS-6.3 scaffolds (Fig. 6C and D). Unlike the results found with the MT-SS-0 and SS-11.8 scaffolds, significantly stronger expression of KDr and Flt-1 appeared on the SS-6.3 scaffolds, following intense immunofluorescent staining of CD31 marker that is associated with vascular endothelial cells [48,49]. These results indicated that silk fibroin scaffolds with improved myogenic or endothelial differentiation capacity could be achieved by a simple lyophilization process.

4. Conclusions

Water-insoluble silk fibroin nanofibrous scaffolds with low β-sheet content were directly prepared from silk fibroin aqueous solution using silk fibroin nanofibers as inducers or nucleators. The stiffness of the scaffolds could be adjusted by tuning the added silk fibroin nanofiber content to match different soft tissues. Stem cells showed different preferred differentiation behavior to muscle and endothelial cells on these scaffolds with tunable stiffness, through the silk fibroin nanofiber-assisted lyophilization process.

Supplementary Material

Refer to Web version on PubMed Central for supplementary material.

Acknowledgments

We thank the National Basic Research Program of China (973 Program 2013CB934400), NSFC (21174097, 81272106) and the NIH (R01 DE017207, P41 EB002520) for support of this work. We also thank the Priority Academic Program Development of Jiangsu Higher Education Institutions (PAPD), the Excellent Youth Foundation of Jiangsu Province (BK2012009), the Natural Science Foundation of Jiangsu Province (Grants No BK20140397), and the Key Natural Science Foundation of the Jiangsu Higher Education Institutions of China (11KGA430002) for support of this work.

References

1. Cukierman E, Pankov R, Stevens DR, Yamada KM. Taking cell-matrix adhesions to the third dimension. Science. 2001; 23:1708–12. [PubMed: 11721053]
2. Abbott A. Cell culture: biology's new dimension. Nature. 2003; 424:870–2. [PubMed: 12931155]
3. Engler AJ, Sen S, Sweeney HL, Discher DE. Matrix elasticity directs stem cell lineage specification. Cell. 2006; 126:677–89. [PubMed: 16923388]
4. Kim HN, Jiao A, Hwang NS, Kim MS, Kang DH, Kim DH, et al. Nanotopography-guided tissue engineering and regenerative medicine. Adv Drug Deliver Rev. 2013; 65:536–58.
5. Huang CC, Ravindran S, Yin Z, George A. 3-D self-assembling leucine zipper hydrogel with tunable properties for tissue engineering. Biomaterials. 2014; 35:5316–26. [PubMed: 24713184]
6. Benoit DSW, Schwartz MP, Durney AR, Anseth KS. Small function groups for controlled differentiation of hydrogel-encapsulated human mesenchymal stem cells. Nat Mater. 2008; 7:816–23. [PubMed: 18724374]
7. Fu J, Wang YK, Yang MT, Desai RA, Yu X, Liu Z, et al. Mechanical regulation of cell function with geometrically modulated elastomeric substrates. Nat Methods. 2010; 7:733–6. [PubMed: 20676108]
8. Hu X, Park SH, Gil ES, Xia XX, Weiss AS, Kaplan DL. The influence of elasticity and surface roughness on myogenic and osteogenic-differentiation of cells on silk-elastin biomaterials. Biomaterials. 2011; 32:8979–89. [PubMed: 21872326]
9. Park JS, Chu JS, Tsou AD, Diop R, Tang Z, Wang A, et al. The effect of matrix stiffness on the differentiation of mysenchymal stem cells in response to TGF-β. Biomaterials. 2011; 32:3921–30. [PubMed: 21397942]
10. Solanki A, Chueng STD, Yin PT, Kappera R, Chhowalla M, Lee KB. Axonal alignment and enhanced neuronal differentiation of neural stem cells on graphene-nanoparticle hybrid structures. Adv Mater. 2013; 25:5477–82. [PubMed: 23824715]
11. Altman GH, Diaz F, Jakuba C, Calabro T, Horan RL, Chen JS, et al. Silk-based biomaterials. Biomaterials. 2003; 24:401–16. [PubMed: 12423595]
12. Wang Y, Bella E, Lee CSD, Migliaresi C, Pelcastre L, Schwartz Z, et al. The synergistic effects of 3-D porous silk fibroin matrix scaffold properties and hydrodynamic environment in cartilage tissue regeneration. Biomaterials. 2010; 31:4672–81. [PubMed: 20303584]
13. Partlow BP, Hanna CW, Rnjak-Kovacina J, Moreau JE, Applegate MB, Burke KA, et al. Highly tunable elastomeric silk biomaterials. Adv Funct Mater. 2014; 24:4615–24. [PubMed: 25395921]
14. Wu J, Rnjak-Kovacina J, Du Y, Funderburgh ML, Kaplan DL, Funderburgh JL. Corneal stromal bioequivalents secreted on patterned silk substrates. Biomaterials. 2014; 35:3744–55. [PubMed: 24503156]
15. McNamara SL, Rnjak-Kovacina J, Schmidt DF, Lo TJ, Kaplan DL. Silk as a biocohesive sacrificial binder in the fabrication of hydroxyapatite load bearing scaffolds. Biomaterials. 2014; 35:6941–53. [PubMed: 24881027]
16. Shao Z, Vollrath F. Surprising strength of silkworm silk. Nature. 2002; 418:741. [PubMed: 12181556]
17. Meinel L, Hofmann S, Karageorgiou V, Kirker-Head C, McCool J, Gronowicz G, et al. The inflammatory responses to silk films in vitro and in vivo. Biomaterials. 2005; 26:147–55. [PubMed: 15207461]

18. Kim HJ, Kim UJ, Vunjak-Novakovic G, Min BH, Kaplan DL. Influence of macroporous protein scaffolds on bone tissue engineering from bone marrow stem cells. Biomaterials. 2005; 26:4442–52. [PubMed: 15701373]
19. Jiang C, Wang X, Gunawidjaja R, Lin YH, Gupta MK, Kaplan DL, et al. Mechanical properties of robust ultrathin silk fibroin films. Adv Funct Mater. 2007; 17:2229–37.
20. Wang Y, Rudym DD, Walsh A, Abrahamsen L, Kim HJ, Kim HS, et al. In vivo degradation of three-dimensional silk fibroin scaffolds. Biomaterials. 2008; 29:3415–28. [PubMed: 18502501]
21. Higuchi A, Ling QD, Hsu ST, Umezawa A. Biomimetic cell culture proteins as extracellular matrices for stem cell differentiation. Chem Rev. 2012; 112:4507–40. [PubMed: 22621236]
22. Gong P, Zheng W, Huang Z, Zhang W, Xiao D, Jiang X. A strategy for the construction of controlled, three-dimensional, multilayered, tissue-like structures. Adv Funct Mater. 2013; 23:42–6.
23. Lee SS, Huang BJ, Kaltz SR, Sur S, Newcomb CJ, Stock SR, et al. Bone regeneration with low dose BMP-2 amplified by biomimetic supramolecular nanofibers within collagen scaffolds. Biomaterials. 2013; 34:452–9. [PubMed: 23099062]
24. Li A, Hokugo A, Yalom A, Berns EJ, Stephanopoulos N, McClendon MT, et al. A bioengineered peripheral nerve construct using aligned peptide amphiphile nanofibers. Biomaterials. 2014; 35:8780–90. [PubMed: 25064803]
25. Cristalini C, Rocchietti EC, Accomasso L, Folino A, Gallina C, Muratori L, et al. The effect of bioartificial constructs that mimic myocardial structure and biomechanical properties on stem cell commitment towards cardiac lineage. Biomaterials. 2014; 35:92–104. [PubMed: 24099712]
26. Liu H, Li X, Zhou G, Fan H, Fan Y. Electrospun sulfated silk fibroin nanofibrous scaffolds for vascular tissue engineering. Biomaterials. 2011; 32:3784–93. [PubMed: 21376391]
27. Zhang X, Baughman CB, Kaplan DL. In vitro evaluation of electrospun silk fibroin scaffolds for vascular cell growth. Biomaterials. 2008; 29:2217–27. [PubMed: 18279952]
28. Prabhakaran MP, Venugopal JR, Ramakrishna S. Mesenchymal stem cell differentiation to neuronal cells on electrospun nanofibrous substrates for nerve tissue engineering. Biomaterials. 2009; 30:4996–5003. [PubMed: 19539369]
29. Meinel AJ, Kubow KE, Klotzsch E, Garcia-Fuentes M, Smith ML, Vogel V, et al. Optimization strategies for electrospun silk fibroin tissue engineering scaffolds. Biomaterials. 2009; 30:3058–67. [PubMed: 19233463]
30. Lu Q, Wang X, Lu S, Li M, Kaplan DL, Zhu H. Nanofibrous architecture of silk fibroin scaffolds prepared with a mild self-assembly process. Biomaterials. 2011; 32:1059–67. [PubMed: 20970185]
31. Coburn JM, Gibson M, Monagle S, Patterson Z, Elisseeff JH. Bioinspired nanofibers support chondrogenesis for articular cartilage repair. Proc Natl Acad Sci USA. 2012; 109:10012–7. [PubMed: 22665791]
32. Rockwood DN, Preda RC, Yucel T, Wang X, Lovett ML, Kaplan DL. Materials fabrication from Bombyx mori silk fibroin. Nat Protoc. 2011; 6:1612–31. [PubMed: 21959241]
33. Yao DY, Dong S, Lu Q, Hu X, Kaplan DL, Zhang BB, et al. Salt-leached silk scaffolds with tunable mechanical properties. Biomacromolecules. 2012; 13:3723–9. [PubMed: 23016499]
34. Liu S, Dong C, Lu G, Lu Q, Li Z, Kaplan DL, et al. Bilayered vascular grafts based on silk proteins. Acta Biomater. 2013; 9:8991–9003. [PubMed: 23851155]
35. Kim UJ, Park J, Kim HJ, Wada M, Kaplan DL. Three-dimensional aqueous-derived biomaterial scaffolds from silk fibroin. Biomaterials. 2005; 26:2775–85. [PubMed: 15585282]
36. Nazarov R, Jin HJ, Kaplan DL. Porous 3-D scaffolds from regenerated silk fibroin. Biomacromolecules. 2004; 5:718–26. [PubMed: 15132652]
37. Jin HJ, Park J, Karageorgiou V, Kim UJ, Valluzzi R, Cebe P, et al. Water-stable silk films with reduced -sheet content. Adv Funct Mater. 2005; 15:1241–7.
38. Lu Q, Zhu H, Zhang C, Zhang F, Zhang B, Kaplan DL. Silk self-assembly mechanisms and control from thermodynamics to kinetics. Biomacromolecules. 2012; 13:826–32. [PubMed: 22320432]
39. Bai S, Liu S, Zhang C, Xu W, Lu Q, Han H, et al. Controllable transition of silk fibroin nanostructures: An insight into in vitro silk self-assembly process. Acta Biomater. 2013; 9:7806–13. [PubMed: 23628774]

40. Lin SS, Lu GZ, Liu SS, Bai SM, Liu X, Lu Q, et al. Nanoscale control of silks for nanofibrous scaffold formation with an improved porous structure. J Mater Chem B. 2014; 2:2622–33.
41. Lu GZ, Liu SS, Lin SS, Kaplan DL, Lu Q. Silk porous scaffolds with nanofibrous microstructures and tunable properties. Colloid Surface B. 2014; 120:28–37.
42. Han F, Liu S, Liu X, Pei Y, Bai S, Zhao H, et al. Woven silk fabric-reinforced silk nanofibrous scaffolds for regenerating load-bearing soft tissues. Acta Biomater. 2014; 10:921–30. [PubMed: 24090985]
43. Bai S, Zhang X, Lu Q, Sheng W, Liu L, Dong B, et al. Reversible hydrogel-solution system of silk with high beta-sheet content. Biomacromolecules. 2014; 15:3044–51. [PubMed: 25056606]
44. Bai SM, Zhang WM, Lu Q, Ma QH, Kaplan DL, Zhu HS. Silk nanofiber hydrogels with tunable modulus to regulate nerve stem cell fate. J Mater Chem B. 2014; 2:6590–600.
45. Sun J, Wei D, Zhu Y, Zhong M, Zuo Y, Fan H, et al. A spatial patternable macroporous hydrogel with cell-affinity domains to enhance cell spreading and differentiation. Biomaterials. 2014; 35:4759–68. [PubMed: 24636216]
46. Wingate K, Bonani W, Tan Y, Bryant SJ, Tan W. Compressive elasticity of three-dimensional nanofiber matrix directs mesenchymal stem cell differentiation to vascular cells with endothelial or smooth muscle cell markers. Acta Biomater. 2012; 8:1440–9. [PubMed: 22266031]
47. Valarmathi MT, Davis JM, Yost MJ, Goodwin RL, Potts JD. A three-dimensional model of vasculogenesis. Biomaterials. 2009; 30:1098–112. [PubMed: 19027154]
48. Dunne LW, Iyyanki T, Hubenak J, Mathur AB. Characterization of dielectrophoresis-aligned nanofibrous silk fibroin-chitosan scaffold and its interactions with endothelial cells for tissue engineering applications. Acta Biomater. 2014; 10:3630–40. [PubMed: 24821141]
49. Huang NF, Okogbaa J, Lee JC, Jha A, Zaitseva TS, Paukshto MV, et al. The modulation of endothelial cell morphology, function, and survival using anisotropic nanofibrillar collagen scaffolds. Biomaterials. 2013; 34:4038–47. [PubMed: 23480958]
50. Wu X, Hou J, Li M, Wang J, Kaplan DL, Lu S. Sodium dodecyl sulfate-induced rapid gelation of silk fibroin. Acta Biomater. 2012; 8:2185–92. [PubMed: 22406911]
51. Mathur AB, Collinsworth AM, Reichert WM, Kraus WE, Truskey GA. Endothelial, cardiac muscle and skeletal muscle exhibit different viscous and elastic properties as determined by atomic force microscopy. J Biomech. 2001; 34:1545–53. [PubMed: 11716856]
52. Song Y, Ju Y, Song G, Morita Y. *In vitro* proliferation and osteogenic differentiation of mesenchymal stem cells on nanoporous alumina. Int J Nanomedicine. 2013; 8:2745–56. [PubMed: 23935364]
53. Florczyk SJ, Kim DJ, Wood DL, Zhang M. Influence of processing parameters on pore structure of 3D porous chitosan-alginate polyelectrolyte complex scaffolds. J Biomed Mater Res A. 2011; 98:614–20. [PubMed: 21721118]
54. Zoldan J, Karagiannis ED, Lee CY, Anderson DG, Langer R, Levenberg S. The influence of scaffold elasticity on germ layer specification of human embryonic stem cells. Biomaterials. 2011; 32:9612–21. [PubMed: 21963156]
55. Pek YS, Wan ACA, Ying JY. The effect of matrix stiffness on mesenchymal stem cell differentiation in a 3D thixotropic gel. Biomaterials. 2010; 31:385–91. [PubMed: 19811817]
56. Toma C, Pittenger MF, Cahill KS, Byrne BJ, Kessler PD. Human mesenchymal stem cells differentiate to a cardiomyocyte phenotype in the adult murine heart. Circulation. 2002; 105:93–8. [PubMed: 11772882]
57. Bardouille C, Lehmann J, Heimann P, Jockusch H. Growth and differentiation of permanent and secondary mouse myogenic cell lines on microcarriers. Appl Microbiol Biot. 2001; 55:556–62.
58. Peloquin J, Huynh J, Williams RM, Reinhart-King CA. Indentation measurements of the subendothelial matrix in bovine carotid arteries. J Biomech. 2011; 44:815–21. [PubMed: 21288524]

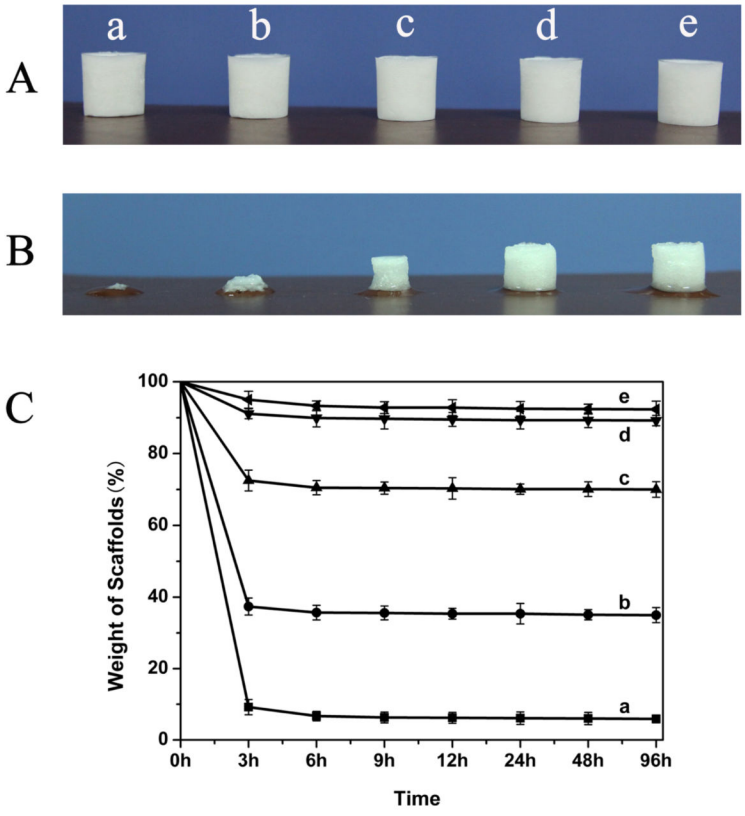

Fig. 1.

The stability of the silk fibroin scaffolds with different contents of silk fibroin nanofibers before (A) and after water immersion for 12 h at 37°C (B). (C) Weight curves of silk fibroin scaffolds after water immersion for different times at 37°C : (a)SS-0, silk fibroin nanofiber content 0%; (b) SS-2, silk fibroin nanofiber content 2%; (c) SS-6.3, silk fibroin nanofiber content 6.3%; (d) SS-11.8, silk fibroin nanofiber content 11.8%; (e) SS-33.3, silk fibroin nanofiber content 33.3%.

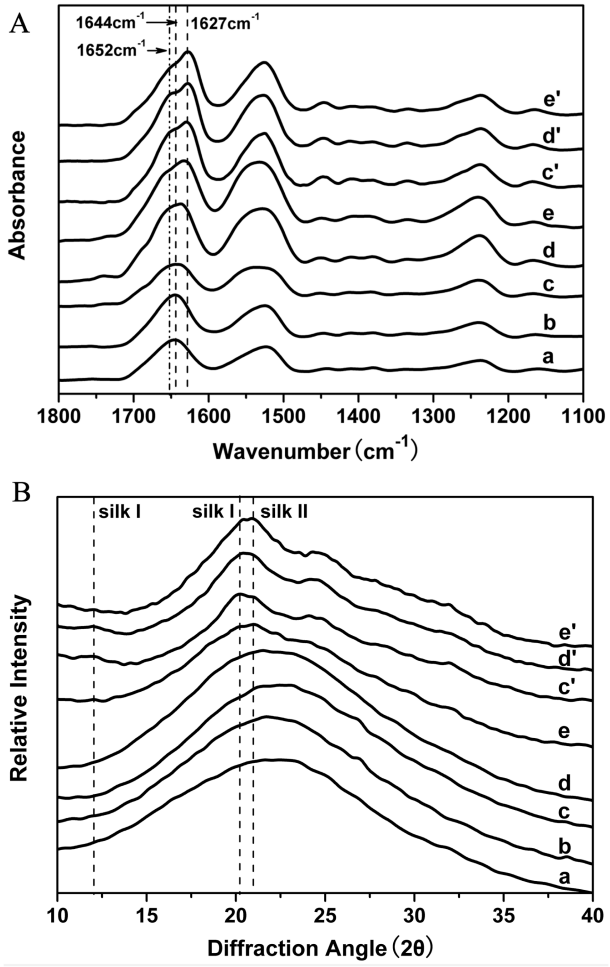

Fig. 2.

FTIR spectra (A) and XRD curves (B) of silk fibroin scaffolds with different contents of silk fibroin nanofibers before (a-e) and after water immersion treatment (c′-e′): (a)SS-0, silk fibroin nanofiber content 0%; (b) SS-2, silk fibroin nanofiber content 2%; (c) SS-6.3, silk fibroin nanofiber content 6.3%; (d) SS-11.8, silk fibroin nanofiber content 11.8%; (e) SS-33.3, silk fibroin nanofiber content 33.3%. The samples (c′-e′) are the corresponding scaffolds of samples (c-e) after water immersion treatment.

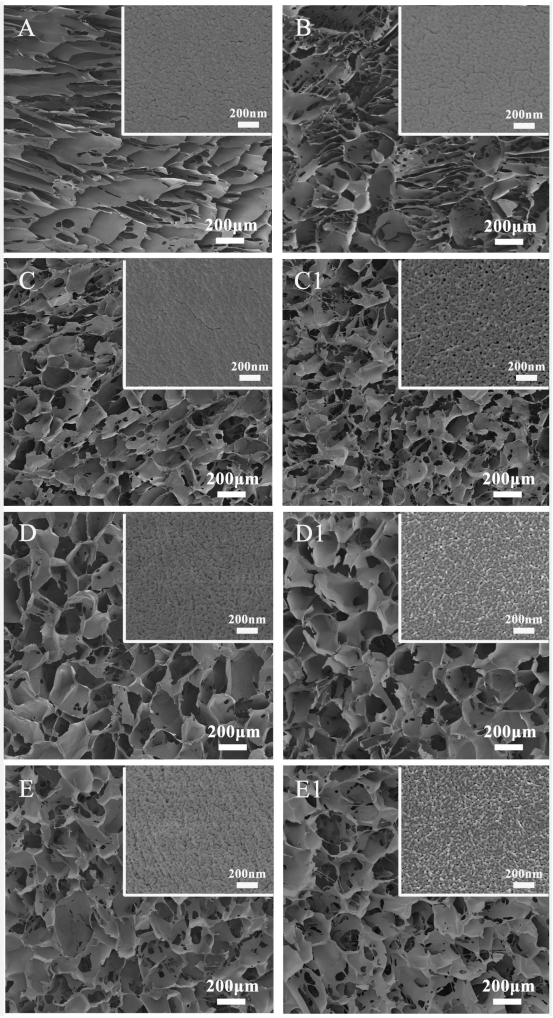

Fig. 3.

SEM morphologies of silk fibroin scaffolds with different contents of silk fibroin nanofibers before (A-E) and after water immersion treatment (C1-E1): (A)SS-0, silk fibroin nanofiber content 0%; (B) SS-2, silk fibroin nanofiber content 2%; (C) SS-6.3, silk fibroin nanofiber content 6.3%; (D) SS-11.8, silk fibroin nanofiber content 11.8%; (E) SS-33.3, silk fibroin nanofiber content 33.3%. The samples (C1-E1) are the corresponding scaffolds of samples (C-E) after water immersion treatment. The insert images show the high magnification morphology of the porous walls of the scaffolds.

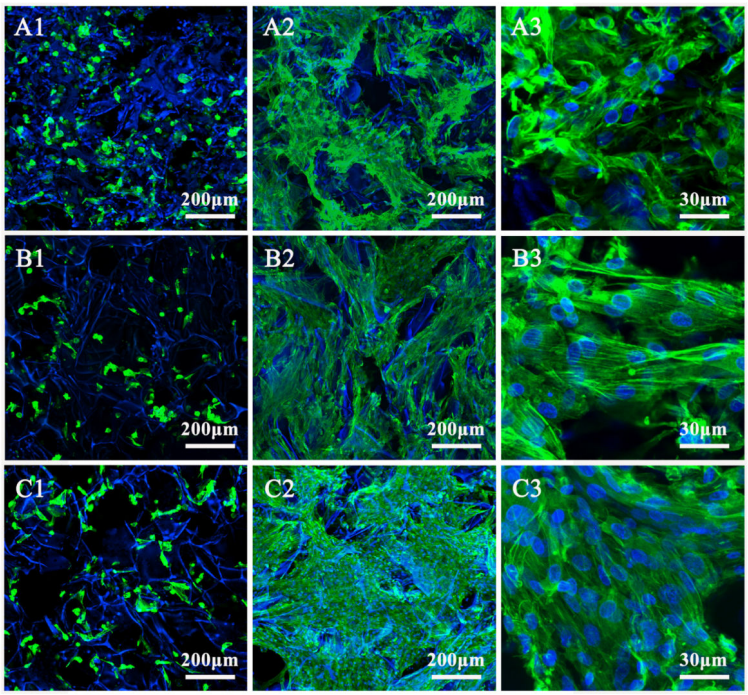

Fig. 4.

Confocal microscopy of BMSCs on different scaffolds at days 1 and 12: (A1) methanol-treated SS-0 scaffolds (MT-SS-0), day 1; (A2) and (A3) methanol-treated SS-0 scaffolds (MT-SS-0), day 12; (B1)SS-6.3 scaffolds, day 1; (B2) and (B3) SS-6.3 scaffolds, day 12; (C1) SS-11.8 scaffolds, day 1; (C2) and (C3) SS-11.8 scaffolds, day 12. The blue color (DAPI) represents silk scaffolds and cell nucleus, while the green color (FITC labeled phalloidin) represents actin cytoskeleton.

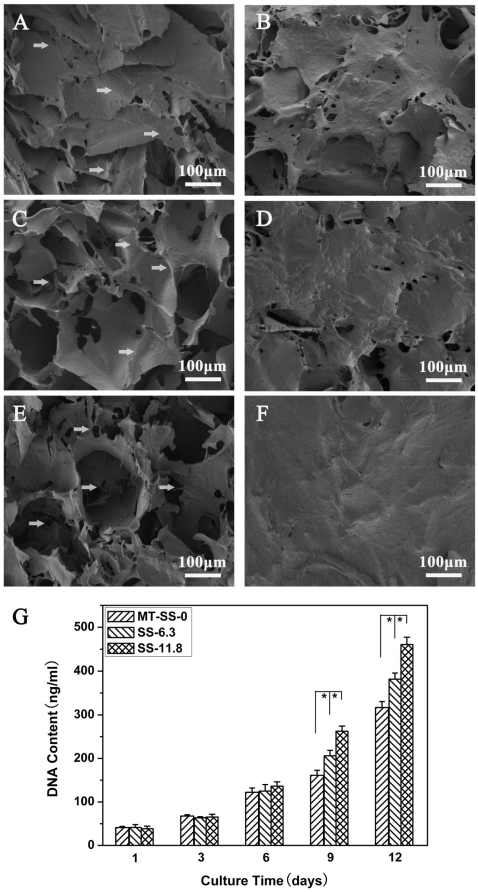

Fig. 5.

SEM images of BMSCs on different scaffolds at day 1 and 12: (A) methanol-treated SS-0 scaffolds, MT-SS-0, day 1; (B) methanol-treated SS-0 scaffolds, MT-SS-0, day 12; (C) SS-6.3 scaffolds, day 1; (D) SS-6.3 scaffolds, day 12; (E) SS-11.8 scaffolds, day 1; (F) SS-11.8 scaffolds, day 12. (G) BMSC proliferation on different silk fibroin scaffolds measured with DNA analysis. *statistically significant $P<0.05$.

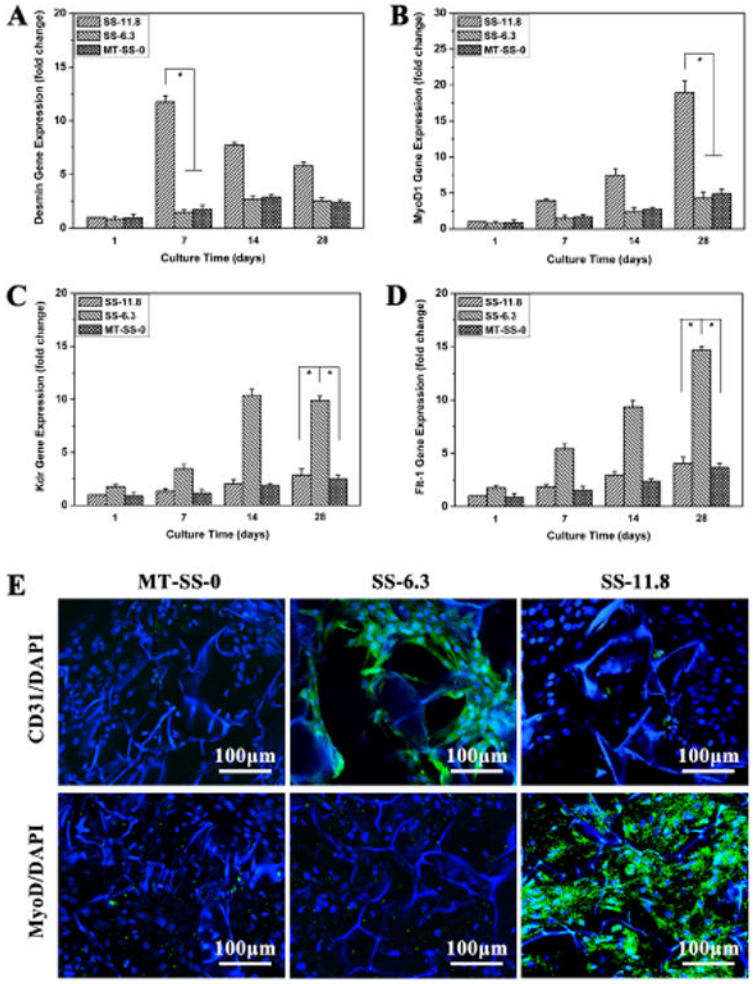

Fig. 6.

Quantitative real-time PCR (qRT-PCR) analysis of selected key differentiation markers. Relative expression levels of Desmin (A), MyoD1 (B), Kdr(C) and Flt-1 (D) for BMSCs cultured on different scaffolds. *statistically significant $P<0.05$. (E) Immunofluorescence micrographs of BMSCs differentiation on different scaffolds with different mechanical properties at day 28. The cells were stained for CD31, and MyoD and DAPI, respectively.

Table 1

Primers used in quantitative real-time PCR (qRT-PCR).

Genes	Primer Sequence (F, R, 5′-3′)	Product Length (bp)
GAPDH	TGGGTGTGAACCACGAGAA	143
	GGCATGGACTGTGGTCATGA	
Desmin	TCCTACACCTGCGAGATTG	116
	GCGATGTTGTCCTGATAGC	
MyoD1	TGGGACATGGAGCTACTATCGC	119
	GGTGAGTCGAAACACGGATCAT	
Kdr	TAAACTAGGCAAATCACTCG	115
	CTCTTTCAACATCTTCACAGC	
Flt-1	CGGAGAAATCTGCTCGCTAT	190
	CTTGGAAGGGACGACACG	

Table 2

The structural conformation ratios in silk fibroin scaffolds derived from deconvoluted amide I FTIR spectra.

Samples[a]	Conformation content of silk fibroin			
	Random	β-Sheet	Silk I (Type II β-turn)	Bends and Turns
SS-0	40.7 ± 3.4	16.6 ±1.7	13.9± 1.6	27.5 ± 2.8
SS-2	35.4 ± 3.2	20.3 ± 1.8	14.7 ± 1.8	27.0 ± 2.6
SS-6.3	30.3 ± 3.1	24.9 ± 2.7	16.5 ± 1.9	25.9 ± 2.4
SS-11.8	26.3 ± 2.0	28.3 ± 2.6	18.7 ± 1.9	23.4 ± 2.3
SS-33.3	22.9 ± 2.2	32.3 ± 3.1	20.1 ± 2.0	21.2 ± 2.1
SS-6.3[b]	16.4 ± 1.7	38.8 ± 2.1	26.6 ± 2.1	16.2 ± 1.8
SS-11.8[b]	15.2 ± 1.8	42.5 ± 2.4	21.4 ± 2.3	17.4 ± 1.6
SS-33.3[b]	15.4 ± 1.4	46.9 ± 3.3	17.4 ± 1.9	16.8 ± 1.8

[a] Ten measurements per condition were obtained.

[b] Water-insoluble silk nanofibrous scaffolds.

Table 3

Mechanical properties of silk scaffolds in wet conditions.

	SS-6.3[a]	SS-11.8[a]	SS-33.3[a]	MT-SS-0[b]
Modulus (kPa)	6.2 ± 0.6	16.7 ± 1.3	5.1 ± 1.5	24.6± 2.1

[a] Water-insoluble silk nanofibrous scaffolds;

[b] MT means methanol treatment.